Magnetism and magnetocaloric effect of single-crystal Er$_5$Si$_4$ under pressure

N. Marcano,[1,2,3] P. A. Algarabel,[1,2] J. Rodríguez Fernández,[4] C. Magén,[2,5,6] L. Morellón,[1,2,5] Niraj K. Singh,[7] D. L. Schlagel,[7] K. A. Gschneidner Jr.,[7,8] V. K. Pecharsky,[7] and M. R. Ibarra[1,2,5]

[1]*Departamento Física de la Materia Condensada, Universidad de Zaragoza, ES-50009 Zaragoza, Spain*
[2]*Instituto de Ciencia de Materiales de Aragón, CSIC-Universidad de Zaragoza, ES-50009 Zaragoza, Spain*
[3]*Centro Universitario de la Defensa, Academia General Militar Crta. Huesca s/n, ES-50090 Zaragoza, Spain*
[4]*Departamento CITIMAC, Universidad de Cantabria, ES-39005 Santander, Spain*
[5]*Instituto de Nanociencia de Aragón, Universidad de Zaragoza, ES-50018 Zaragoza, Spain*
[6]*Fundación ARAID, ES-50004 Zaragoza, Spain*
[7]*Ames Laboratory, U. S. Department of Energy, Iowa State University, Ames, Iowa 50011-3020, USA*
[8]*Department of Materials Science and Engineering, Iowa State University, Ames, Iowa, 50011-2030, USA*

Magnetic and magnetocaloric properties of single-crystalline Er$_5$Si$_4$ have been investigated as a function of the applied magnetic field (up to 50 kOe) and the hydrostatic pressure (up to 10 kbar) in the 5–300 K temperature range along the three main crystallographic directions. The magnetization isotherms show a highly anisotropic behavior with the easy-magnetization direction along the b axis for the low-pressure monoclinic and high-pressure orthorhombic structures, in good agreement with previous neutron scattering experiments. Below T_C, the approach to the saturation shows a steplike behavior when the magnetic field is applied along the hard directions. The steps are sharper as the pressure increases. At constant magnetic field change, increasing the pressure induces a highly anisotropic enhancement of the magnetic entropy change. An enhancement of 20% is observed along the easy axis b, where the magnetic entropy change is maximum. The different evolution of the magnitude and temperature dependence of the magnetocaloric effect along the three crystallographic directions with pressure is discussed.

I. INTRODUCTION

The effect of the hydrostatic pressure on the magnetic and structural properties of the $R_5(\text{Si}_x\text{Ge}_{1-x})_4$ (with $R =$ rare earth) compounds has been deeply explored over the last few years in order to get a better understanding of the interplay between the crystal structure and magnetism in this family of intermetallic compounds (see review in Ref. 1). Many of these alloys show a strong magnetostructural coupling manifested in the existence of magnetic and structural transitions that can be reversibly induced by modifying one or more external parameters such as temperature, magnetic field, or hydrostatic pressure. As a consequence, many interesting effects have been discovered in this family of compounds: giant magnetocaloric effect,[2] large magnetoresistance,[3] and giant magnetostriction[4] are only a few examples. The physical properties of the 5:4 family are governed by their peculiar crystal structures, which are intrinsically layered and are formed by the stacking of very stable two-dimensional layers (slabs) of R and Si/Ge atoms.[5] The crystallographic phase and magnetic ordering are controlled by the number of interlayer covalentlike Si/Ge-Si/Ge bonds connecting the slabs.[6] Therefore, the hydrostatic pressure allows us to control the distance and bonding between slabs, being a key parameter to determine the crystallographic and magnetic states in these alloys. Three main crystal structures are present in this family of compounds, the crystal symmetry of which is controlled by the interslab distance and Si(Ge)-Si(Ge) bonding. The Gd$_5$Si$_4$ type [so-called O(I) state] crystallizes in orthorhombic *Pnma* space group and it is characterized by conserving all the Si(Ge)-Si(Ge) pairs covalently bonded. When half of the bonds are broken, this system presents a Gd$_5$Si$_2$Ge$_2$-type monoclinic $P112_1/a$

symmetry (the M phase). Eventually, the system recovers the orthorhombic *Pnma* symmetry when all pairs are unbonded, crystallizing in the so-called O(II) phase.

Among all of the 5:4 compounds studied, the Er$_5$Si$_4$ shows the most outstanding behavior under hydrostatic pressure and will be the subject of study in this work. Er$_5$Si$_4$ exhibits a Gd$_5$Si$_4$-type [O(I) state with space group *Pnma*] crystal structure at room temperature, and on cooling it undergoes a first-order crystallographic phase transition to a Gd$_5$Si$_2$Ge$_2$-type crystal structure (M state, space group $P112_1/a$) in the paramagnetic state at a characteristic temperature $T_t \sim$ 200–230 K.[7,8] The system becomes ferromagnetic (FM) at low temperature, $T_C = 30$ K.[7,9–11] Further studies by means of neutron scattering[8,12] indicated a complex noncollinear ferromagnetic state below T_C with an easy magnetization direction along the b axis. A weak antiferromagnetic coupling was observed in the (010) plane, with Er moments forming small canting angles with the b direction. Those studies also revealed that no structural change accompanies the magnetic ordering at low temperature and ambient pressure.

Recent studies have shown that a high magnetic field induces a structural transformation to the orthorhombic phase, giving rise to the O(I) FM phase at low temperatures ($H > 80$ kOe at $T = 5$ K).[13,14] On the other hand, hydrostatic pressure not only induces the O(I) phase at low temperature, but also shifts the high-temperature crystallographic change at a very high rate of $dT_t/dP \sim -30$ K/kbar.[15] This causes both transitions (the high-temperature crystallographic and the low-temperature magnetic ordering) to collapse at high pressures (above 6 kbar), which stabilizes the O(I) Er$_5$Si$_4$ over the whole temperature range, maximizing the magnetocaloric

effect at low temperature.[16] This low-temperature O(I) crystal structure has a Curie temperature $T_C^{O(I)} = 35$ K, higher than that of the monoclinic phase $T_C^M = 30$ K.

The studies mentioned above have been performed on polycrystalline samples where some aspects of the physical behavior may be masked or averaged out, mainly those associated with anisotropic properties. Remarkable anisotropic magnetic properties have been observed in different members of the family based on Gd (Refs. [17–20]) and Tb,[21–23] even in the case of 5:4 single crystals based on Gd ($L = 0$). The study of other compounds of the family with nonzero rare-earth orbital momentum is necessary to understand the origin of magnetocrystalline anisotropy in these compounds and its relevance in the magnetocaloric properties. The use of hydrostatic pressure in these materials has demonstrated to be an interesting approach to analyze the coupling between the crystal structure and the magnetism.[1,15,16,20,24–27] Thus, the aim of this work is to investigate the magnetic properties of single-crystalline Er_5Si_4 under hydrostatic pressure. We have performed a complete study of the magnetic properties along the main crystallographic directions by measuring the magnetization, up to an applied magnetic field of 50 kOe, as a function of the temperature and the hydrostatic pressure. From these measurements, the magnetocaloric effect (MCE) along the different crystallographic directions has been calculated, and its dependence on the hydrostatic pressure and magnetic field determined. The strong anisotropic character of the Er^{3+} will be reflected in the complex magnetic behavior observed in the isothermal magnetization curves and also in the difference of the MCE along the different crystallographic directions.

II. EXPERIMENTAL DETAILS

A large single crystal of Er_5Si_4 was grown by the Bridgman method[28] from stoichiometric amounts of high-purity Er prepared by the Materials Preparation Center of the Ames Laboratory[29] and silicon. Purities of the starting components were identical to that described in Ref. [11]. The as-grown crystal was oriented by back-reflection Laue technique, and the crystallographic directions assigned using scans on a conventional x-ray powder diffractometer. A sample in the shape of a parallelepiped (1.40 mm × 0.80 mm × 0.48 mm) was cut by spark erosion and the faces were polished using standard metallographic techniques.

Magnetic measurements were performed in a commercial (Quantum Design) superconducting quantum interference device (SQUID) magnetometer in applied magnetic fields up to 50 kOe in the temperature range 2–300 K. Pressure experiments were carried out using a miniature piston-cylinder-type CuBe pressure cell by Quantum Design. The applied pressure was estimated from the superconducting critical temperature using a Sn manometer. The sample and the Sn manometer were compressed in a Teflon capsule filled with a liquid pressure-transmitting medium (a mixture of mineral oils). Technical details about the pressure cell can be found in Ref. [30]. The magnetization was measured under hydrostatic pressures up to 10 kbar. The magnetic entropy change ΔS_{mag} has been calculated numerically following the well-known

expression

$$\Delta S_{\mathrm{mag}}(T,H,P) = \int_0^H \left[\frac{\partial M(T,H,P)}{\partial T} \right]_H dH \qquad (1)$$

derived by integration of the Maxwell relation $(\partial S/\partial H)_T = (\partial M/\partial T)_H$.[31,32]

III. RESULTS AND DISCUSSION

Low-temperature magnetization isotherms have been measured at selected hydrostatic pressures ranging from 0 to ∼10 kbar (values at low temperatures) along the three crystallographic directions. Figure 1 illustrates the measurements carried out at 5 K. These results clearly show that the b axis is the easy magnetization axis at $T = 5$ K [Fig. 1(b)] and the a direction is the hard magnetization axis [Fig. 1(a)], whereas the c direction appears to be an intermediate situation. From the saturation magnetization and the strong magnetic anisotropy observed, it is evident that the system at ambient pressure is not a simple ferromagnet at low temperatures. The magnetization along the b axis [Fig. 1(b)] shows a rapid increase at low fields associated with domain-wall movement. After that, the magnetization reaches the saturation giving rise to a saturation magnetization value of $M_s = 195$ emu/g at 50 kOe, which yields a magnetic moment of $6.4\mu_B$ per Er atom (far from the expected value for the saturation magnetization of $gJ = 9\mu_B$/Er). The shape and the magnitude of the isotherms are remarkably different along the a and c axes. At ambient pressure, several metamagnetic processes take place in magnetic fields between 10 and 30 kOe, each of them followed by a hysteretic behavior. The magnetization at 50 kOe reaches $3.8\mu_B$/Er and $5.8\mu_B$/Er along the a and c directions, respectively, again significantly lower than the theoretical saturation value of $9\mu_B$/Er. These observations are in agreement with the canted ferromagnetic structure characterized by neutron diffraction below $T_C = 30$ K (Ref. [8]) with an easy-magnetization axis along the b axis and a weak antiferromagnetic coupling in the (010) plane.

The effect of the applied pressure is remarkably different along the three crystallographic directions. Whereas the general features remain essentially unchanged with applied pressure along the easy-axis [Fig. 1(b)] magnetization, isotherms along the a and c directions [Figs. 1(a) and 1(c)] show a strong change both in the shape and the magnitude of the magnetization when pressure increases up to ∼3.5 kbar after which they remain only weakly affected. This fact indicates that low pressure ($P < 3.5$ kbar) induces a remarkable change in the magnetic state of Er_5Si_4 at 5 K. The application of ∼3.5 kbar makes the metamagneticlike transitions sharper, whereas the hysteretic behavior is suppressed in both cases. Magnetization smoothly increases with the magnetic field reaching $4.4\mu_B$/Er at 50 kOe for the a direction (∼15% higher than the ambient pressure value), whereas along the c axis, magnetization reaches $6\mu_B$/Er at 50 kOe (∼4% higher than the ambient pressure value). It is worth noting that this behavior remains unchanged at higher pressure, so the changes induced by pressure at 5 K along both the a and c axes are already completed at ∼3.5 kbar. From these results, we deduce that although modifications of magnetic and/or crystallographic properties are induced by pressure, ferromagnetic ordering
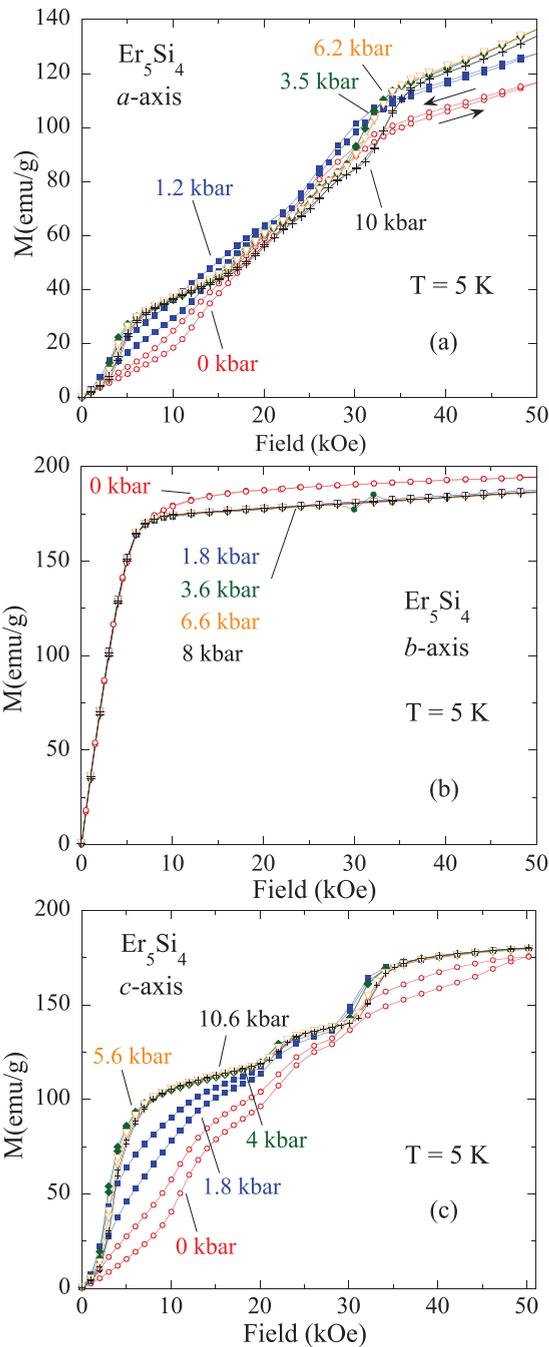
FIG. 1. (Color online) Magnetization isotherms of Er$_5$Si$_4$ measured at 5 K as a function of the hydrostatic pressure with the magnetic field applied along the (a) a, (b) b, and (c) c axes.

FIG. 2. (Color online) Magnetization isotherms of Er$_5$Si$_4$ measured along the three crystallographic axis at selected pressures and temperatures in the vicinity of the magnetic ordering: (a) a axis at 20 K, (b) b axis, and (c) c axis. The inset displays the corresponding isotherms at 40 K.

along the b axis with some canting in the ac plane is still observed at high pressure.

Figure 2 displays the measurements carried out in the vicinity of T_C at 20 and 40 K (corresponding insets) for the three crystallographic directions. At 20 K, the magnetization of the ambient-pressure isotherm measured along the easy axis b [Fig. 2(b)] has decreased due to the proximity of T_C, whereas the magnetization along a and c [Figs. 2(a) and 2(c), respectively] shows a single metamagneticlike transition at about 10 kOe. For all the cases, the 3-kbar isotherm represents a crossover between the low-pressure low-magnetization state

and the high-pressure high-magnetization regime. The latter effect is remarkable along the a and c axes: at maximum field, the high-pressure magnetization values are ~30% higher than those at ambient pressure along both the a and c axes, whereas the magnetization only slightly increases along the b axis (~2.5%). It is remarkable that the increase of the magnetization associated with domain-wall movement observed at low fields along the b direction is more abrupt in the high-pressure regime ($P > 3.5$ kbar), exhibiting a much

more rapid tendency toward saturation. This fact suggests the existence of stronger ferromagnetic correlations at higher hydrostatic pressures.

In the three directions, the pressure-induced changes are completed at $P \geqslant 4$ kbar. At 40 K, the magnetic signal has significantly decreased for the three crystallographic directions. Again, a low-magnetization behavior is observed at low pressures ($P < 2$ kbar) and the ~ 6 kbar measurement displays a greater magnetization value, almost 36%, 20%, and 40% larger than the ambient-pressure signal along the a, b and c axes, respectively [insets of Figs. 2(a), 2(b), and 2(c)]. It is worth noting that the enhancement of the magnetization when pressure increases is stronger along the hard a and c axes. These changes can be understood assuming a change from the M FM state present at ambient pressure to the $O(\mathrm{I})$ FM state at high enough pressure. As was already discussed in the Introduction, magnetic, linear thermal expansion measurements and neutron diffraction experiments have shown that the hydrostatic pressures stabilizes the $O(\mathrm{I})$ FM phase in polycrystalline samples.[15,16] High applied field measurements[14] also evidence that the effect of the magnetic field at low temperatures is to produce a mixture of both phases M FM and $O(\mathrm{I})$ FM, the volume of the $O(\mathrm{I})$ FM phase growing at the expense of the M FM phase as the magnetic field increases. We propose a similar scenario to explain the magnetization measurements under hydrostatic pressure in the single crystal: at ambient pressure, the magnetization measurements correspond to the M FM phase and at high enough applied pressure, the magnetization is associated with the $O(\mathrm{I})$ FM behavior. At intermediate pressure, both phases coexist, and the magnetization presents an intermediate behavior, increasing the relative volume of the $O(\mathrm{I})$ phase as the pressure is increased. The applied pressure at which the complete transformation takes place depends on temperature. At 5 K, ~ 3.5 kbar is enough to complete the transformation to the high-pressure phase. Once the whole volume of the sample corresponds to the $O(\mathrm{I})$ FM phase, no more changes in the magnetic behavior are observed. For 20 and 40 K, the pressure needed to complete the transformation increases to ~ 4 and ~ 5.5 kbar, respectively.

The complex approach to the saturation observed when the magnetic field is applied along the hard directions is associated to the energy-level splitting produced by crystal electric field (CEF) acting on the Er^{3+} ions. It is worth noting that the M phase has five independent Er sites. Two pairs of these sites are semi-independent since they are formed by splitting of two eightfold sites in the $O(\mathrm{I})$ structure.[5] Assuming a single-ion model, we can explain the multiple steps on the magnetization isotherms as associated with the spin reorientation in the different sets of Er sites due to the fact that the applied magnetic field produces a crossing of the CEF levels in each site.[33,34] The complex crystallographic structure and high number of different sites for the Er^{3+} ions makes very difficult a theoretical calculation using a CEF-based Hamiltonian due to the large number of parameters present in such CEF Hamiltonian. It is worth noting the existence of magnetic anisotropy even at 40 K in the paramagnetic phase (see inset of Fig. 2), which is a well-known feature of rare-earth intermetallics as, for instance, in RNi_5 alloys.[35]
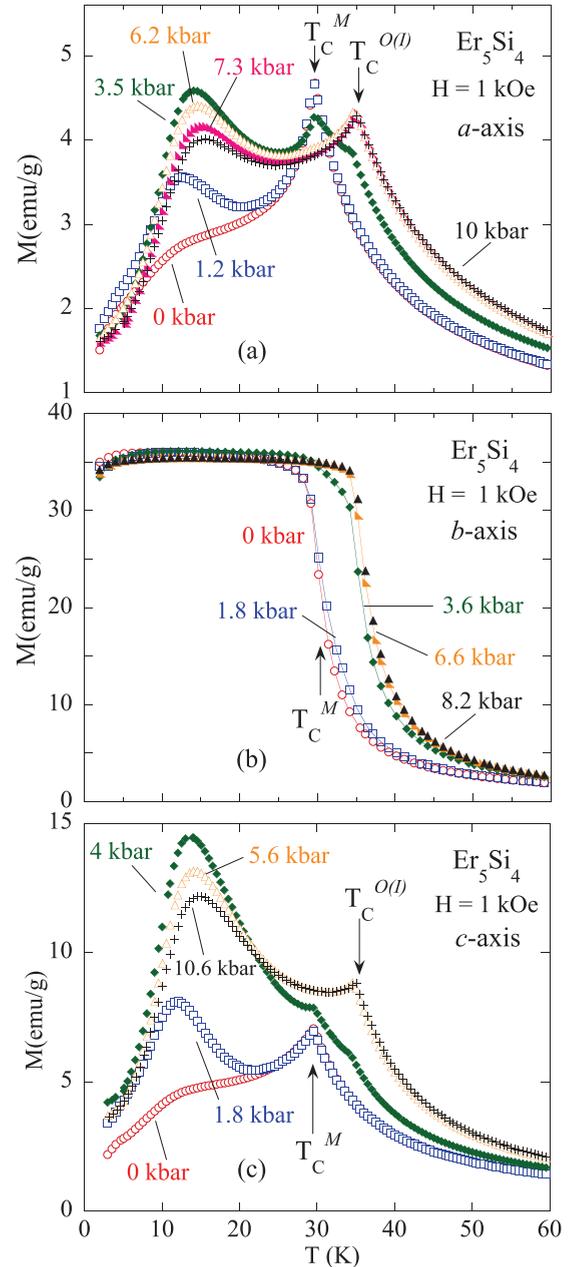
FIG. 3. (Color online) Magnetization of Er_5Si_4 as a function of temperature and hydrostatic pressure measured during heating in 1 kOe magnetic field applied along the a, b, and c axes. The ordering temperatures of the two polymorphic modifications of Er_5Si_4 are marked with arrows.

Temperature-dependent magnetization measurements under hydrostatic pressure have been performed with the magnetic field applied along the a, b, and c axes of the crystal, and these are shown for $H = 1$ kOe and different pressures in Fig. 3. Measurements have been carried out on heating after cooling in zero field. At ambient pressure, the FM ordering of the M crystallographic phase of Er_5Si_4 appears as a marked peak at $T_C^M = 30$ K along the a and c axes and a sharp anomaly along the b axis, where T_C^M is determined as the maximum of the derivative $|(\frac{dM}{dT})_H|$. In addition, a low-temperature anomaly ($T \sim 10$–20 K) is observed for

the a and c axes, which is related to a spin reorientation characterized by neutron diffraction around $\sim$15 K.[8] The effect of the pressure on the magnetization is different along the three crystallographic directions. For the easy axis [Fig. 3(b)], a low-pressure transition ($P < 2$ kbar) is observed around 30 K and a high-pressure transition ($P > 2$ kbar) occurs around 35 K, which correspond to T_C^M and $T_C^{O(I)}$, respectively. For the a and c axes, however, the application of pressure induces two apparently independent processes, similarly to the behavior reported for polycrystalline specimens of Er_5Si_4 (Ref. [14]): on the one hand, the growth of the low-temperature anomaly ($T\sim$ 10–20 K), which shifts toward higher temperature values and gradually broadens as pressure increases, and, on the other hand, the appearance of a new peak at $T_C^{O(I)} \sim 35$ K. It is worth noting, however, that both pressure-induced processes are remarkably different along the a and c axes. First, the contribution of the peak at $T_C^{O(I)}$ gradually increases, while the anomaly at T_C^M progressively disappears along the a axis [Fig. 3(a)] resembling the behavior of the polycrystalline sample. However, along the c axis, this increment at $T_C^{O(I)}$ occurs while the anomaly at T_C^M progressively increases [Fig. 3(c)]. For both crystallographic directions, the anomaly at $T_C^{O(I)}$ becomes dominant at $\sim$6 kbar and the peak at T_C^M nearly disappears. Second, the low-temperature anomaly reaches much greater magnetization values with the magnetic field applied along the c axis than the a axis. The magnetization value for the former is nearly a factor 3 at the highest pressure value $\sim$10 kbar. The observed change from T_C^M to $T_C^{O(I)}$ can be explained with the physical picture of an equilibrium state where two phases with different ordering temperatures coexist at intermediate pressures.[15] The increasing pressure reduces the concentration of the monoclinic phase with $T_C^M = 30$ K, which is stable at ambient pressure, and transforms it into a new orthorhombic phase with $T_C^{O(I)} = 35$ K, which becomes dominant at pressures over 6 kbar. The unexpected increase at low pressures of the magnitude of the anomaly at $T_C^M = 30$ K observed along c does not contradict this picture if we consider the extent of the broad low temperature peak associated with the spin reorientation transition. This broad anomaly increases spectacularly upon pressure, and this increase can easily account for the observed enhancement of the T_C^M peak, when the expected tendency in this scenario would be a reduction due to the lower concentration of the M FM phase.

Figure 4 displays the high-field magnetization measurements ($H = 10$ kOe) along the three crystallographic directions in the vicinity of the low-temperature magnetic transitions. For each case, the ambient-pressure measurements resemble the low-field curves shown in Fig. 3 with an obviously higher magnetic signal. A pressure of $\sim$3.5 kbar induces a significant increase of the low-temperature magnetization along the a [Fig. 4(a)] and c [Fig. 4(c)] axes, which is nearly three times the ambient-pressure value along the c axis, whereas no remarkable change is observed along the b axis [Fig. 4(b)]. Higher pressure does not significantly increase the maximum magnetization value in each case, which resembles the saturation of the pressure effects observed in the magnetization isotherms. The anomaly near T_C diminishes with pressure along the c axis, whereas along the a axis the
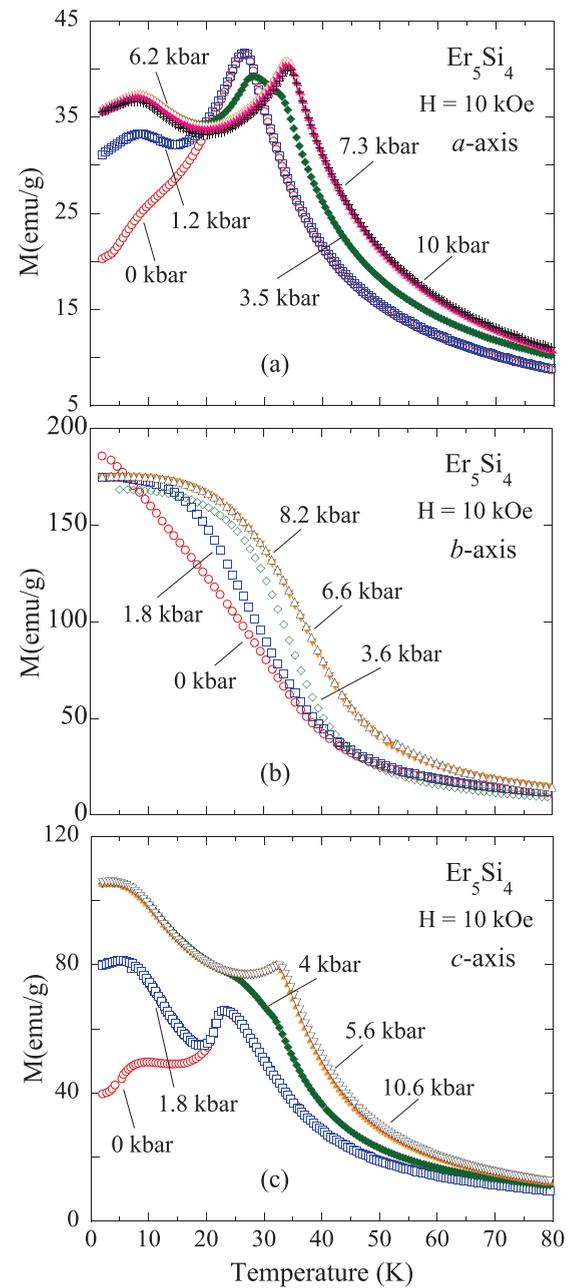
FIG. 4. (Color online) Temperature dependence of the high-field magnetization of Er_5Si_4 in the vicinity of the low-temperature magnetic ordering measured during heating at selected pressures in a 10-kOe magnetic field along the a, b, and c axes.

pressure shifts the anomaly toward higher temperatures, and the magnetization value at the maximum remains unaffected by the pressure. In the latter case, at intermediate pressures ($P = 3.5$ kbar), a new anomaly appears close to 35 K ($T_C^{O(I)}$), the contribution of which gradually increases with rising pressure, while the anomaly at T_C^M progressively diminishes. At higher pressure ($P > 7$ kbar), the anomaly at $T_C^{O(I)}$ becomes dominant, but the peak at T_C^M has disappeared.

These results indicate that the hydrostatic pressure induces remarkable changes in the magnetic state of Er_5Si_4, although different effects are seen along different crystallographic directions. The increase of the magnetization signal at low

temperature can be interpreted as the favoring of a more collinear FM structure, whereas a higher T_C could be related to stronger FM interactions. These observations are related to shortening of the interslab distances, causing the onset of the $O(\mathrm{I})$ crystallographic structure, as reported in polycrystalline Er_5Si_4 at low temperature with the application of a magnetic field and hydrostatic pressure.[14,15]

The structural $O(\mathrm{I}) \longleftrightarrow M$ transformation in the paramagnetic regime, which is detected by an observable change of slope in the magnetization,[7] significantly shifts to low temperatures with increasing pressure for the three crystallographic directions. The high-temperature structural-only transition is shown for the a axis in Fig. 5 as representative of this study. A steplike anomaly is observed in the magnetization between ~212 and ~154 K on warming and a similar anomaly occurs between the same both temperatures on cooling. There is a large thermal hysteresis between the warming and the cooling magnetization curves. The width of thermal hysteresis amounts to about 50 K at ambient pressure. This observation agrees with previous work on the polycrystalline sample,[15] which reported a gradual and extended first-order transformation.[7,8] In the present case, however, the crystallographic transition spans a larger temperature range. Under pressure, the steplike anomaly becomes smoother: at 1.2 kbar [see Fig. 5(b)], the beginning of the thermal hysteresis T_t^*, which defines the extended first-order structural transformation, shifts from ~212 down to ~160 K. At 3.6 kbar, it shifts down to ~100 K [see Fig. 5(c)]. Such a displacement is equivalent to a rate $dT_t^*/dP \approx -26$ K/kbar. This value is similar to the 23-K/kbar value obtained from the magnetization measurements in the polycrystalline sample.[15] By contrast, the thermal hysteresis ($\Delta T \approx 50$ K) remains unaffected with applied pressure, whereas the steplike anomaly in the magnetization, which defines the structural transition, becomes smoother. This fact introduces uncertainty in the determination of the transition temperature at high pressures.

Several sets of magnetization isotherms have been measured at different pressures in the temperature range from 5 to 70 K in order to calculate the magnetic entropy change along the three crystallographic directions. The magnetic entropy changes (ΔS_{mag}) calculated using Eq. (1) from the magnetization isotherms are shown in Fig. 6 for a magnetic field change $\Delta H = 20$ kOe in Figs. 6(a), 6(b), and 6(c). Different features are observed in the MCE curves with pressure for the three crystallographic directions. The evolution of the magnitude and the temperature of the MCE peak for the easy-axis direction [see Fig. 6(b)] resemble the behavior reported for the polycrystalline sample.[16] The magnitude of the MCE increases with pressure from 8.5 J/kg K at ambient pressure up to 10.5 J/kg K at 1.8 kbar with the peak value remaining at a constant temperature of $T \sim 30$ K, which corresponds to T_C^M [Fig. 6(b)]. As pressure increases, the MCE moves to higher temperature and its maximum increases in its magnitude, reaching a value of $\Delta S_{\mathrm{mag}} \sim 12$ J/kg K at 8 kbar and $T \sim 35$ K, which coincides with $T_C^{O(\mathrm{I})}$, giving rise to a 41% enhancement of the MCE peak at the magnetic field change of 20 kOe with respect to ambient pressure. This value is slightly lower than that reported for the polycrystalline sample (56%).
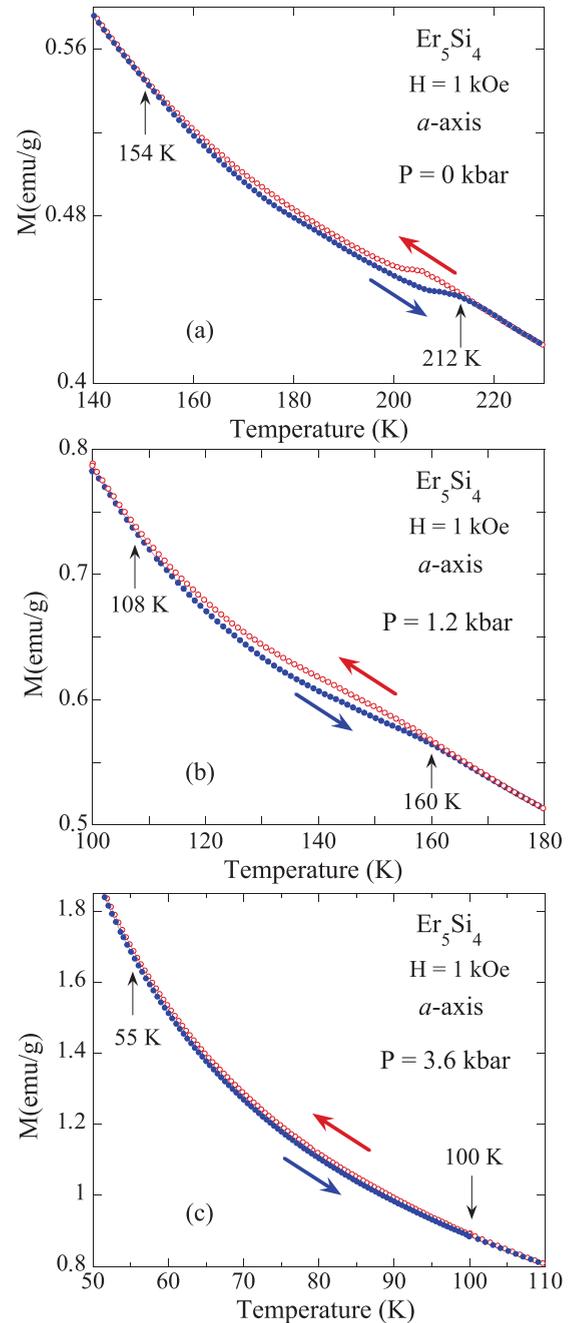
FIG. 5. (Color online) Pressure dependence of the magnetization in the proximity of the structural transition measured in 1-kOe magnetic field along the a direction. Open symbols are used for the cooling curves and filled symbols are for the heating runs. The different curves are labeled with the corresponding pressure values. The vertical arrows indicate the beginning and the end of the thermal hysteresis. Note the different scales in temperature.

The magnetic entropy change calculated for the a and c axes presents common features when applying pressure, although different from those described above for the easy axis. Thus, the magnitude of the peak in MCE increases with pressure, although the values involved in these cases are much lower than those found along the b axis: the MCE increases from 2.9 J/kg K at ambient pressure with the peak at ~32 K up to 3.1 J/kg K at 9.7 kbar at $T \sim 37$ K along the a axis [Fig. 6(a)],
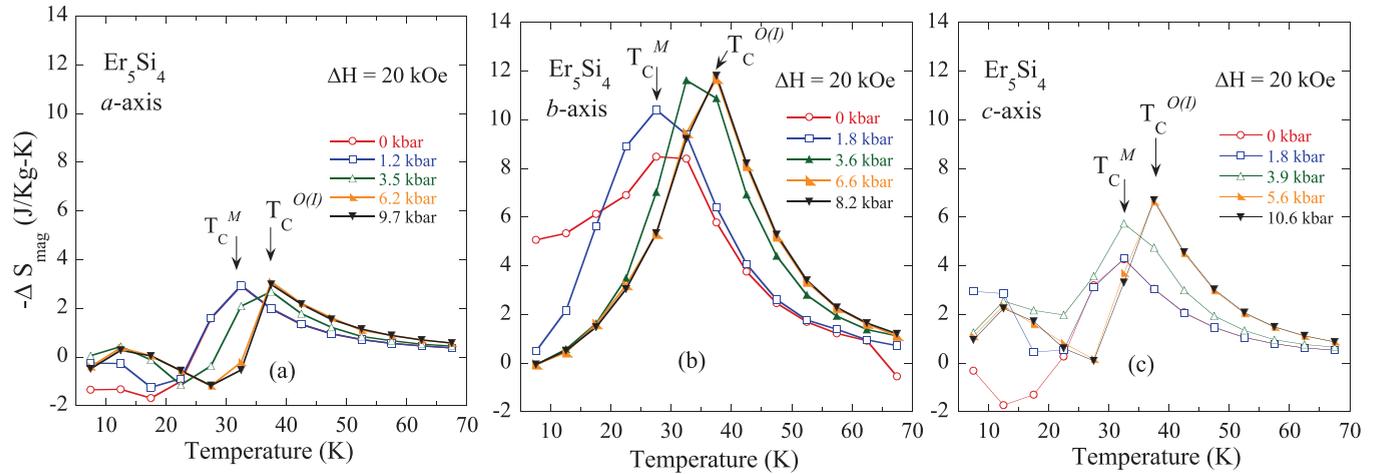
FIG. 6. (Color online) Magnetocaloric effect of Er_5Si_4 at different pressures calculated for a magnetic field change $\Delta H = 20$ kOe along the (a) a, (b) b, and (c) c axes.

whereas along the c axis, the increment goes from 4.2 J/Kg K at ambient pressure up to 6.7 J/kg K at 10.6 kbar [Fig. 6(c)]. The overall increase in MCE is 7% and 60% for the a and c axes, respectively. For both directions, a negative MCE is observed below 20 K, giving rise to a broad negative shoulder at ambient pressure. Such a shoulder becomes less pronounced as pressure is applied, turning into a positive shoulder for pressures above ∼1.5 kbar. With a magnetic field change of 50 kOe, the evolution of the MCE peak with pressure is similar to $\Delta H = 20$ kOe (not shown). On the other hand, the low-temperature shoulder observed for the a and c axes at ambient pressure is not present.

The main features displayed by the MCE curves (i.e., the pressure dependencies of the maximum value of ΔS_{mag} for the a, b, and c axes at a magnetic field change $\Delta H = 50$ kOe) are plotted in Fig. 7. The peak value of MCE saturates at 1.8 kbar for the easy axis b. This saturation occurs at some pressure value between 3.5 and 6 kbar for the a and c axes. The overall increase in MCE is 41% for both axes, which is higher
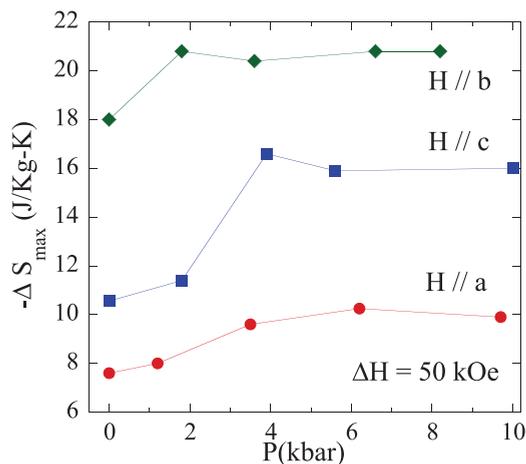
than the corresponding MCE increase with pressure along the b axis (∼17%). It is worth noting that the increase of MCE reported for the polycrystalline sample (35%) nearly doubles that observed in the easy axis of the single-crystalline sample in this work. The values of MCE at ambient pressure in the latter case, however, are higher than the corresponding values in the polycrystalline sample.

The dependence of the MCE with the direction at which the magnetic field is applied reflects the strong anisotropic character of the Er^{3+} ion and the pressure dependence of the MCE is associated with pressure-induced $M \rightarrow O(I)$ structural transformation that takes place in Er_5Si_4. When the magnetic field is applied along the easy-magnetization direction (b axis), the MCE shows a normal behavior with a maximum at the ordering temperature. At ambient pressure, the maximum occurs at 30 K, corresponding to the Curie temperature of the M FM phase T_C^M. As the hydrostatic pressure is increased, the maximum shifts to 37 K, corresponding to the Curie temperature of the $O(I)$ FM phase $T_C^{O(I)}$. At pressures $\geqslant 6.6$ kbar, the behavior of the MCE remains unchanged, indicating that the transformation is complete in the whole temperature range. An intermediate behavior between the ambient-pressure M FM behavior and the high $O(I)$ FM behavior is observed for an intermediate range of pressures, reflecting again the phase coexistence. The enhancement of the MCE in the $O(I)$ FM phase is associated with stronger ferromagnetic correlations due to the modification of the interlayer coupling between the M and $O(I)$ states. In the high-pressure $O(I)$ phase, all of the covalentlike interslab bonds are formed, favoring the ferromagnetic interlayer interactions.[6,36]

The complex approach to the saturation observed in the magnetic isotherms when the magnetic field is applied along the hard directions is reflected in the temperature dependence of the MCE presented in Fig. 6. The MCE shows a peak at the ordering temperature, changing from 30 K (M phase) to 37 K [$O(I)$ phase], but below 30 K the MCE shows a nonmonotonic behavior with even negative values (inverse MCE). Such a behavior is associated with the strong magnetocrystalline anisotropy of the Er^{3+} ion, which produces a reduction of the magnetization at 5 K with respect to that measured at higher

FIG. 7. (Color online) Maximum value of the magnetic entropy change for a magnetic field change $\Delta H = 50$ kOe along the a, b, and c axes as a function of the hydrostatic pressure.

temperatures (see Figs. 1 and 2) due to steplike approach to the saturation at low temperatures.

IV. CONCLUSIONS

A study of the magnetization in a wide range of temperatures, magnetic field, and hydrostatic pressure has been performed for a single crystal of Er_5Si_4 with the magnetic field applied along the main crystallographic directions. The experimental measurements confirm the b axis as the easy-magnetization direction and show a complex, steplike approach to the saturation at low temperatures when the magnetic field is applied along the hard magnetic directions. The magnetization results have been explained assuming the existence of pressure-induced transformation from the low-pressure M phase to a high-pressure $O(I)$ phase. At intermediate pressures, coexistence of both crystallographic phases has been detected.

Using the Maxwell relation, ΔS_{mag} has been calculated with the magnetic field applied along three main crystallographic directions as a function of applied magnetic field and hydrostatic pressure. ΔS_{mag} shows a normal behavior when the magnetic field is applied along the easy-magnetization direction with a maximum observed at the magnetic ordering temperature. When the magnetic field is applied along the hard direction, ΔS_{mag} shows a complex behavior, with inverse MCE at low temperatures, originated by the strong magnetocrystalline anisotropy of the Er^{3+} ion. The MCE results have been explained assuming a phase transformation and an enhancement of the ferromagnetic correlations in the $O(I)$ phase compared with the M phase. The study of the anisotropic effects of MCE in Er_5Si_4 as a function of pressure reveals that the effect of pressure is remarkable in the c axis, whereas

in the easy-magnetization b axis is quite moderate and an intermediate situation occurs in the hardest a axis. The small difference between the MCE as a function of pressure along the easy axis with respect to the polycrystal suggests that textured Er_5Si_4 does not provide a major improvement in terms of absolute MCE with the aim of application. On the other hand, texturing can be a possible strategy in order to choose the optimal crystal orientation to obtain a large differential MCE if hydrostatic pressure is the tuning parameter. This idea should be explored by further analysis of MCE as a function of pressure in single crystals with even higher anisotropy in order to elucidate the interest of this approach. For instance, previous analysis carried out in single-crystalline $Tb_5Si_{2.2}Ge_{1.8}$ shows that the strong single-ion anisotropy of Tb gives rise to huge anisotropy in both magnetization [in this case, the easy axis is a, and hardest axis is b with a 1000% relative variation of the MCE (Ref. 37)]. In this system, a much higher differential MCE as a function of pressure should be expected thanks to the combined effect of much larger anisotropy and the recoupling of the magnetic and structural transitions.

[1] C. Magén, L. Morellón, P. A. Algarabel, M. R. Ibarra, Z. Arnold, and C. Ritter, *Advances In Solid State Physics* (Springer, Berlin, 2007), Vol. 46, pp. 241–253.

[2] V. K. Pecharsky and K. A. Gschneidner Jr., Phys. Rev. Lett. **78**, 4494 (1997).

[3] L. Morellón, J. Stankiewicz, B. García-Landa, P. A. Algarabel, and M. R. Ibarra, Appl. Phys. Lett. **73**, 3462 (1998).

[4] L. Morellón, P. A. Algarabel, M. R. Ibarra, J. Blasco, B. García-Landa, Z. Arnold, and F. Albertini, Phys. Rev. B **58**, R14721 (1998).

[5] V. K. Pecharsky and K. A. Gschneidner Jr., Pure Appl. Chem. **79**, 1383 (2007).

[6] W. Choe, V. K. Pecharsky, A. O.Pecharsky, K. A. Gschneidner Jr., V. G. Young Jr., and G. J. Miller, Phys. Rev. Lett. **84**, 4617 (2000).

[7] V. K. Pecharsky, A. O. Pecharsky, Y. Mozharivskyj, K. A. Gschneidner Jr., and G. J. Miller, Phys. Rev. Lett. **91**, 207205 (2003).

[8] C. Ritter, C. Magén, L. Morellón, P. A. Algarabel, M. R. Ibarra, V. K. Pecharsky, A. O. Tsokol, and K. A. Gschneidner Jr., J. Phys.: Condens. Matter **18**, 3937 (2006).

[9] A. M. Pereira, J. P. Araújo, M. E. Braga, R. P. Pinto, J. Ventura, F. C. Correia, J. M. Teixeira, J. B. Sousa, C. Magén, P. A. Algarabel, L. Morellón, and M. R. Ibarra, J. Alloys Compd. **423**, 66 (2006).

[10] F. Holtzberg, R. J. Gambino, and T. R. McGuire, J. Phys. Chem. Solids **28**, 2283 (1967).

[11] Y. Mozharivskyj, A. O. Pecharsky, V. K. Pecharsky, G. J. Miller, and K. A. Gschneidner Jr., Phys. Rev. B **69**, 144102 (2004).

[12] J. M. Cadogan, D. H. Ryan, Z. Altounian, X. Liu, and I. P. Swainson, J. Appl. Phys. **95**, 7076 (2004).

[13] A. O. Pecharsky, K. A. Gschneidner Jr., V. K. Pecharsky, D. L. Schlagel, and T. A. Lograsso, Phys. Rev. B **70**, 144419 (2004).

[14] C. Magén, C. Ritter, L. Morellón, P. A. Algarabel, M. R. Ibarra, A. O. Tsokol, K. A. Gschneidner Jr., and V. K. Pecharsky, Phys. Rev. B **74**, 174413 (2006).

[15] C. Magén, L. Morellón, Z. Arnold, P. A. Algarabel, C. Ritter, M. R. Ibarra, J. Kamarad, A. O. Tsokol, K. A. Gschneidner Jr., and V. K. Pecharsky, Phys. Rev. B **74**, 134427 (2006).

[16] Z. Arnold, C. Magén, L. Morellón, P. A. Algarabel, J. Kamarad, M. R. Ibarra, V. K. Pecharsky, and K. A. Gschneidner Jr., Phys. Rev. B **79**, 144430 (2009).

[17] M. Nazih, A. De Visser, L. Zhang, O. Tegus, and E. Brück, Solid State Commun. **126**, 255 (2003).

[18] H. Tang, A. O. Pecharsky, D. L. Schlagel, T. A. Lograsso, V. K. Pecharsky, and K. A. Gschneidner Jr., J. Appl. Phys. **93**, 8298 (2003).

[19]M. Han, D. C. Jiles, J. E. Snyder, T. A. Lograsso, and D. L. Schlagel, J. Appl. Phys. **95**, 6945 (2004).

[20]C. Magén, L. Morellón, P. A. Algarabel, M. R. Ibarra, Z. Arnold, J. Kamarad, T. A. Lograsso, D. L. Schlagel, V. K. Pecharsky, A. O. Tsokol, and K. A. Gschneidner Jr., Phys. Rev. B **72**, 024416 (2005).

[21]M. Zou, V. K. Pecharsky, K. A. Gschneidner Jr., D. L. Schlagel, and T. A. Lograsso, Phys. Rev. B **78**, 014435 (2008).

[22]M. Zou, V. K. Pecharsky, K. A. Gschneidner Jr., Ya. Mudryk, D. L. Schlagel, and T. A. Lograsso, Phys. Rev. B **80**, 174411 (2009).

[23]A. P. Ring, H. L. Ziegler, T. A. Lograsso, D. L. Schlagel, J. E. Snyder, and D. C. Jiles, J. Appl. Phys. **99**, 08R104 (2006).

[24]C. Magén, Z. Arnold, L. Morellón, Y. Skorokhod, P. A. Algarabel, M. R. Ibarra, and J. Kamarad, Phys. Rev. Lett. **91**, 207202 (2003).

[25]L. Morellón, Z. Arnold, C. Magén, C. Ritter, O. Prokhnenko, Y. Skorokhod, P. A. Algarabel, M. R. Ibarra, and J. Kamarad, Phys. Rev. Lett. **93**, 137201 (2004).

[26]L. Morellón, Z. Arnold, P. A. Algarabel, C. Magén, M. R. Ibarra, and Y. Skorokhod, J. Phys.: Condens. Matter **16**, 1623 (2004).

[27]S. Vélez, J. M. Hernández, A. Fernández, F. Macià, C. Magén, P. A. Algarabel, J. Tejada, and E. M. Chudnovsky, Phys. Rev. B **81**, 064437 (2010).

[28]D. L. Schlagel, T. A. Lograsso, A. O. Pecharsky, and J. A. Sampaio, in *Light Metals 2005*, edited by H. Kvande (The Minerals, Metals and Materials Society, TMS, Warrendale, PA, 2005), p. 1177.

[29]Materials Preparation Center, The Ames Laboratory, US Department of Energy, Ames, IA, USA [http://www.mpc.ameslab.gov].

[30][www.qdusa.com/products/high-pressure-cell-mpms].

[31]A. M. Tishin, in *Handbook of Magnetic Materials*, edited by K. H. J. Buschow (North-Holland, Amsterdam, 1999), Vol. 12, Chap. 4, p. 395.

[32]A. M. Tishin and Y. I. Spichking, *The Magnetocaloric Effect and its Applications* (IOP, Bristol, 2003).

[33]Z. A. Kazei, V. V. Snegirev J.-M. Broto, H. Rakoto, and L. P. Kozeev, Zh. Éksp. Teor. Fiz. **84**, 519 (2006) [JETP Lett. **84**, 441 (2006)].

[34]K. Sugiyama, T. Yamamoto, N. Nakamura, A. Thamizhavel, S. Yoshii, K. Kindo, N. H. Luong, and Y. Onuki, Phys. B (Amsterdam) **327**, 423 (2003).

[35]L. Morellón, P. A. Algarabel, M. R. Ibarra, A. del Moral, D. Gignoux, and D. Schmitt, J. Magn. Magn. Mater. **153**, 17 (1996).

[36]V. K. Pecharsky and K. A. Gschneidner Jr., Adv. Mater. **13**, 683 (2001).

[37]M. Zou, Ya. Mudryk, V. K. Pecharsky, K. A. Gschneidner Jr., D. L. Schlagel, and T. A. Lograsso, Phys. Rev. B **75**, 024418 (2007).